

# Dynamics of Ferroelectric Negative Capacitance - Electrostatic MEMS Hybrid Actuators

Raghuram.T.R<sup>1, a)</sup> and Arvind Ajoy<sup>1, b)</sup>

Department of Electrical Engineering, Indian Institute of Technology Palakkad, Palakkad, India

We propose a framework to model ferroelectric negative capacitance - electrostatic Micro Electro Mechanical Systems (MEMS) hybrid actuators and analyze their dynamic (step input) response. Using this framework, we report the first proposal for reduction in the dynamic pull-in and pull-out voltages of the hybrid actuators due to the negative capacitance of the ferroelectric. The proposed model also reveals the effect of ferroelectric thickness on the dynamic pull-in and pull-out voltages and the effect of ferroelectric damping on the energy dissipated during actuation. We infer from our analysis that the hybrid actuators are better than the standalone MEMS actuators in terms of operating voltage and energy dissipation. Further, we show that one can trade-off a small part of the reduction in actuation voltage to achieve identical pull-in times in the hybrid and standalone MEMS actuators, while still consuming substantially lower energy in the former as compared to the latter. The circuit compatibility of the proposed hybrid actuator model makes it suitable for analysis and evaluation of various heterogeneous systems consisting of hybrid MEMS actuators and other electronic devices.

## I. INTRODUCTION

Micro Electro Mechanical Systems (MEMS) based on electrostatic actuation and sensing are an integral part of today's electronics. The ITRS roadmap describes the significance of many such devices in applications ranging from consumer - to - automotive - to - medical electronics<sup>1</sup>. Electrostatic MEMS actuators are very popular and are widely used because of their inherent low power consumption. The response of such electrostatic MEMS actuators to voltage excitation is different for static and dynamic inputs. The former corresponds to the input voltage being varied slowly, so that the actuator is in quasi-static equilibrium<sup>2-4</sup>. The latter corresponds to the input voltage being varied suddenly, as in the case of a step voltage excitation<sup>2-7</sup>. It is well known that the dynamic response is different from the static response – for example, the dynamic pull-in voltage of a MEMS cantilever is  $0.919 \times$  its static pull-in voltage<sup>2,6</sup>.

The operating voltage of electrostatic MEMS actuators, for

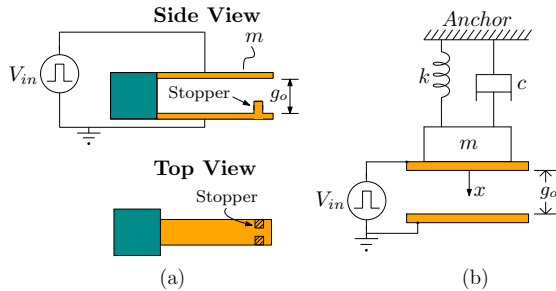


FIG. 1. An example of modeling a generic electrostatic MEMS actuator using a 1-DOF model. (a) Cantilever MEMS (b) Equivalent 1-DOF model capturing the essential features of the cantilever structure.

both static and dynamic inputs, is typically much larger than the supply voltage used in modern CMOS (Complementary Metal Oxide Semiconductor) integrated circuits: 10-100 V as compared to sub-1V CMOS circuit power supplies. Additional on-chip voltage sources and drive electronics are used in present day MEMS-CMOS integrated circuits to meet the high operating voltage requirement of the MEMS actuators<sup>8-11</sup>. Efforts to reduce the operating voltage also involve innovative designs like scaling down the structural parameters such as air-gap  $< 10 \text{ nm}$ <sup>12-14</sup>. Reliable fabrication and operation of MEMS structures with extremely small air-gaps is very challenging due to stiction.

A novel technique to mitigate the demand for high operating voltage of an electrostatic MEMS actuator was proposed in Ref. 15, by connecting a ferroelectric capacitor exhibiting negative capacitance in series with the MEMS actuator, thus forming a hybrid actuator. The "static response" of this hybrid actuator was analyzed in Refs. 15 and 16, where the operating voltage to static inputs was analytically proven to be lowered in the hybrid actuator as compared to the standalone MEMS actuator. The impact of ferroelectric negative capacitance on the energy-delay characteristics of the actuator was theoretically predicted in Ref. 17 – however important effects such as the ferroelectric switching delay and the dependence of electrostatic force on displacement have been ignored therein.

The dynamic response of electrostatic MEMS actuators to step inputs play a key role in switching (like RF MEMS switches) and display applications<sup>18-20</sup>. The dynamic response of hybrid actuators has not been analyzed in the literature. Our work deals with (a) numerical modeling of the hybrid actuator by solving the non-linear differential equations governing its dynamics, (b) investigating its "dynamic response" to a step input, (c) analyzing the effect of ferroelectric parameters on the dynamic response, (d) studying the trade-off between pull-in time and operating voltage and its implication on energy dissipation in the hybrid actuator. We use SPICE (Simulation Program with Integrated Circuit Emphasis) to solve the differential equations mentioned above. SPICE is a popular tool for circuit analysis. Hence our ap-

<sup>a)</sup>Electronic mail: 121704004@smail.iitpkd.ac.in

<sup>b)</sup>Electronic mail: arvindajoy@iitpkd.ac.in

proach leads to a model that can be included seamlessly to evaluate the performance of CMOS-MEMS hybrid circuits.

This paper is organized as follows. Section II reviews the dynamics of a standalone electrostatic MEMS actuator. Section III presents the modeling of the ferroelectric negative capacitance - electrostatic MEMS hybrid actuator. Simulation results and discussion are detailed in section IV. Section V presents our conclusion.

## II. REVIEW OF DYNAMICS OF ELECTROSTATIC MEMS ACTUATOR

In this work, we model a generic standalone electrostatic MEMS actuator as a single degree of freedom (1-DOF) parallel plate arrangement consisting of a pair of electrodes separated by an air-gap  $g_o$ . As shown in the Fig. 1, one electrode (bottom) is fixed and the other (top) is movable. The parameters used in the 1-DOF model (mass  $m$ , spring constant  $k$ , damping coefficient  $c$ ) represent their effective equivalents in the generic actuator. We set the damping coefficient to zero, so as to enable a comparison with analytical results wherever possible. For dynamic operation, a step voltage is applied to the actuator. Below a certain value of this applied step voltage, called the dynamic pull-in voltage, the response of the actuator is periodic. The maximum value of this periodic displacement of the electrode is called dynamic pull-in displacement. When the applied step voltage is larger than the dynamic pull-in voltage, the movable top electrode snaps down onto the bottom electrode. This condition is called dynamic pull-in<sup>5</sup>. After achieving pull-in, when the applied step voltage is decreased to a specific value, called the dynamic release voltage / pull-out voltage, the pull-in condition is lost and the movable top electrode gets detached from the fixed bottom electrode. This condition is termed as release / pull-out. We assume that the MEMS actuator has a pair of stoppers with height  $h_s$ , as shown in Fig. 1(a), to minimize the area of contact upon pull-in and thus minimize the effect of surface forces. We hence neglect these forces in our analysis.

The equation of motion governing the actuator response to the applied voltage  $V_{in} u(t)$ , where  $u(t)$  is the unit step function, is given by

$$m \frac{d^2x}{dt^2} + c \frac{dx}{dt} + kx = \frac{\epsilon_o A_M V_{in}^2}{2(g_o - x)^2} \quad (1)$$

for  $t \geq 0$ .  $A_M$  is the area of the electrode,  $\epsilon_o$  is the permittivity of free space, and  $x$  is the dynamic variable representing the displacement of the electrode. With damping neglected, the dynamic pull-in voltage  $V_{DPI}$ , the dynamic pull-in displacement  $X_{DPI}$  and pull-out voltage  $V_{DPO}$  are given by<sup>4</sup>

$$V_{DPI} = \sqrt{\frac{kg_o^3}{4\epsilon_o A_M}}; X_{DPI} = \frac{g_o}{2}; V_{DPO} = \sqrt{\frac{2kh_s^2(g_o - h_s)}{\epsilon_o A_M}} \quad (2)$$

As a reference, the respective static pull-in quantities are<sup>2</sup>

$$V_{SPI} = \sqrt{\frac{8kg_o^3}{27\epsilon_o A_M}}; X_{SPI} = \frac{g_o}{3}; V_{SPO} = V_{DPO} \quad (3)$$

## III. MODELING FERROELECTRIC NEGATIVE CAPACITANCE - ELECTROSTATIC MEMS HYBRID ACTUATOR

SPICE is a general purpose circuit simulation program for nonlinear DC, nonlinear transient and linear AC analysis. SPICE<sup>22</sup> is used as a modeling program to mathematically predict the behavior of electronic circuits. Although SPICE was originally developed for electronic circuit simulation, it has been extended for design and analysis of problems in various areas of physics – thermal, electro-thermal<sup>23,24</sup>, optics<sup>25,26</sup>, mechanics<sup>27</sup>, biological<sup>28</sup> and microfluidics<sup>29</sup>. Here we use SPICE to numerically solve the differential equations governing the actuator dynamics. This involves using arbitrary voltage sources, current sources and built-in integrate and differentiate functions available in SPICE. Using SPICE to model the actuator is advantageous as SPICE is circuit compatible and thus, the model can be used with other electronic devices to evaluate various heterogeneous systems for different applications.

The SPICE model of the standalone electrostatic MEMS is implemented as shown in Fig. 2, based on Ref. 21. It consists of four modules namely the actuator, the suspension, the Equation Of Motion (EOM) solver and the anchor. These modules are represented as sub-circuits in the schematic along with their associated parameters as depicted in Fig. 2. See [supplementary material](#) for implementation details. The initial displacement and velocity of the movable electrode are taken as zero. The actuator module takes the applied step voltage  $V_{in}$ , area  $A_M$ , initial air-gap  $g_o$  and the electrode displacement  $x_{elec}$  as input parameters and calculates the electrostatic force  $F_{elec} = \epsilon_o A_M V_{in}^2 / 2(g_o - x)^2$ . The suspension module takes the electrode displacement  $x_{elec}$ , electrode velocity  $v_{elec}$ , the spring constant  $k$  and the damping coefficient  $c$  as the input parameters and calculates the mechanical restoring force  $F_{mech} = c \cdot dx/dt + kx$ . The EOM solver module is placed between the actuator and suspension modules. The EOM solver compares the two forces  $F_{elec}$  and  $F_{mech}$  and calculates the acceleration as  $(F_{elec} - F_{mech})/m$  according to Eq.(1). The acceleration is then integrated to obtain the velocity, which is further integrated to obtain the displacement. Feedback connections are provided within these blocks to determine the electrode displacement for an applied voltage. Note that non-electrical quantities are modeled using currents or voltages – suitable conversion factors are therefore required in order to read the final results with appropriate units.

The dynamics of the ferroelectric capacitor (single domain) is captured by the time dependent Landau - Khalatnikov (LK) equation<sup>30-35</sup> relating the voltage  $V_F$  across the ferroelectric to charge  $Q$  as

$$V_F = -\alpha Q + \beta Q^3 + \gamma Q^5 + R_F \frac{dQ}{dt} \quad (4)$$

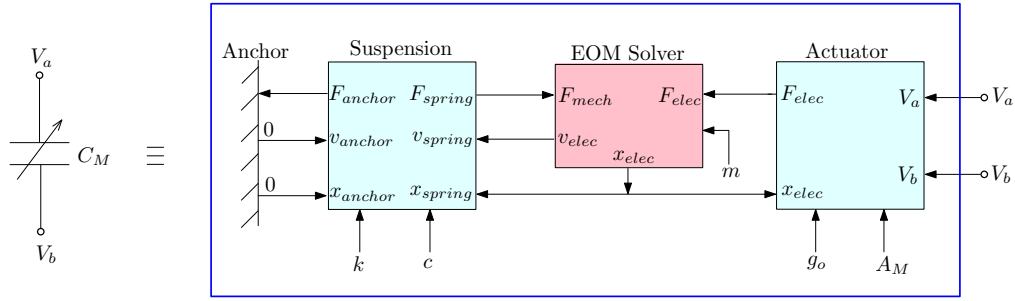


FIG. 2. SPICE model of standalone electrostatic MEMS actuator. Arrows pointing into (out of) a block refer to inputs (outputs) to (from) the block.  $x$  designates position,  $v$  designates velocity and  $F$  designates forces. Implementation of these blocks using circuit elements follows Ref. 21. Refer [supplementary material](#) for detailed schematic implementation.

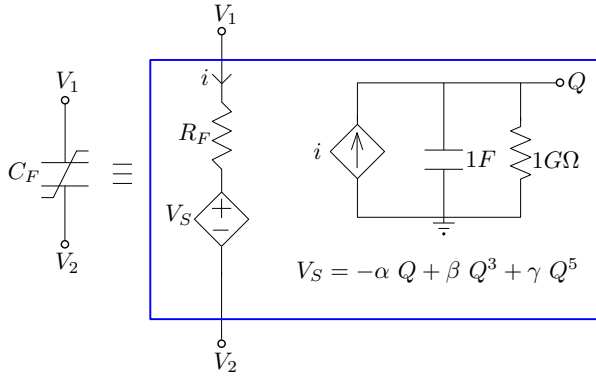


FIG. 3. SPICE model of ferroelectric capacitor. The charge  $Q$  is determined using an RC integrator. The voltage source  $V_S$  is implemented using arbitrary behavioral voltage source in SPICE.

$$\alpha = -\frac{\alpha_F t_F}{A_F}; \beta = \frac{\beta_F t_F}{A_F^3}; \gamma = \frac{\gamma_F t_F}{A_F^5}; R_F = \frac{\rho t_F}{A_F} \quad (5)$$

where  $\rho$  is the ferroelectric damping constant;  $\alpha_F$ ,  $\beta_F$  and  $\gamma_F$  are ferroelectric anisotropy coefficients,  $t_F$ ,  $A_F$  are respectively the thickness and area of the ferroelectric. The last term of Eq.(4) denotes the voltage drop across resistor  $R_F$  with  $dQ/dt$  representing the current  $i$  through it. Thus, Eq. (4) is implemented in SPICE as a Voltage Controlled Voltage Source (VCVS) in series with resistor  $R_F$  <sup>33</sup>. The SPICE model of the ferroelectric capacitor is shown in Fig. 3. The charge  $Q$  is estimated by integrating current  $i$  through the capacitor <sup>36</sup>.

We propose a SPICE model for the ferroelectric negative capacitance - electrostatic MEMS hybrid actuator by cascading the sub-circuit corresponding to the ferroelectric capacitor  $C_F$  with that of the standalone MEMS actuator (depicted as a variable capacitor  $C_M$ ) as shown in Fig. 4. This solves the differential equations Eqs.(1, 4), by ensuring that an identical charge exists on the ferroelectric capacitor and the MEMS actuator.

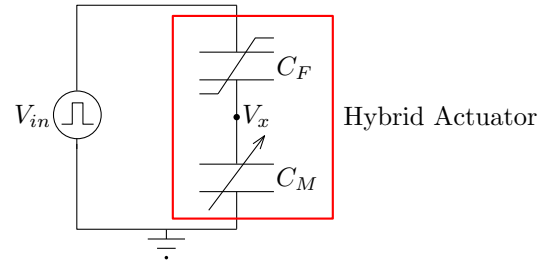


FIG. 4. Ferroelectric negative capacitance -electrostatic MEMS hybrid actuator equivalent circuit.  $C_F$  represents the ferroelectric capacitor and  $C_M$  represents the variable capacitance provided by the MEMS actuator.

#### IV. SIMULATION RESULTS AND DISCUSSION

Table I lists the parameters of the hybrid actuator used in the simulation. SBT ( $\text{Sr}_{0.8}\text{Bi}_{2.2}\text{Ta}_2\text{O}_9$ ) is chosen as the ferroelectric material. The ferroelectric layer thickness and area are designed so as to obtain a static pull-in voltage of 0.80 V and a static pull-out voltage of 0.00 V, using the equations available in Ref. 15. The validation of the SPICE model for static pull-in and pull-out analysis of the hybrid actuator can be found in the [Appendix](#). As mentioned earlier, the movement of the top electrode is limited by means of the stopper of height  $h_s$ .

##### A. Dynamic response of the actuator

Fig. 5 shows the simulated dynamic response of the standalone MEMS actuator. We obtain a dynamic pull-in voltage  $V_{DPI}$  of 18.67 V, a pull-in displacement  $X_{DPI}$  of 1.50  $\mu\text{m}$  and pull-out voltage  $V_{DPO}$  of 17.99 V from the simulation. Our simulation results exactly match with the analytical predictions given by Eq. (2). For input step voltage less than the dynamic pull-in voltage (18.67 V), the actuator response is periodic. For input step voltage greater than the dynamic pull-in voltage, the actuator achieves pull-in. After pull-out, the top electrode oscillates, in the absence of damping.

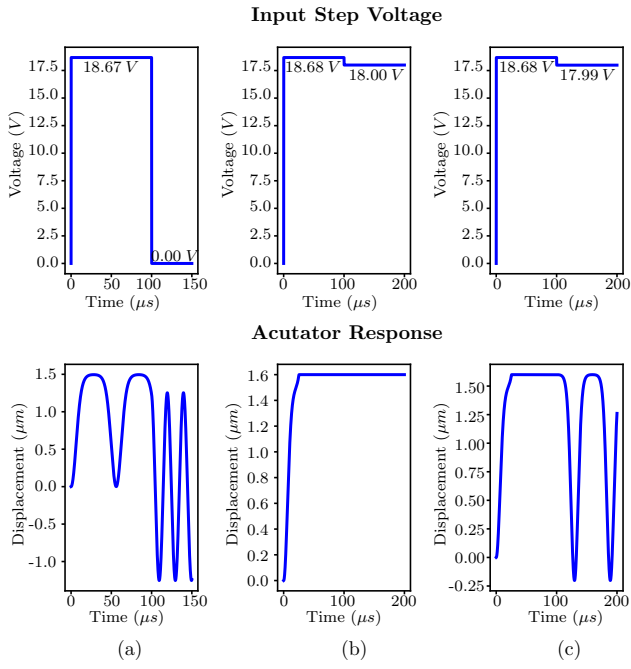


FIG. 5. Standalone electrostatic MEMS actuator dynamic response (a) Actuator response before dynamic pull-in, showing dynamic pull-in displacement  $X_{DPI} = 1.50 \mu\text{m}$ . (b) Actuator response after dynamic pull-in and without release. Note that the stopper restricts the displacement to  $1.6 \mu\text{m}$ . (c) Actuator response after dynamic pull-in and with release. Note that the pull-in voltage  $V_{DPI}$  is  $18.67 \text{ V}$  and release voltage  $V_{DPO}$  is  $17.99 \text{ V}$ .

TABLE I. Ferroelectric negative capacitance - electrostatic MEMS hybrid actuator parameters used for SPICE simulation

Parameter	Value
Length of the cantilever, $L$	$160 \mu\text{m}$
Width of the cantilever, $W$	$6 \mu\text{m}$
Thickness of the cantilever, $T$	$2 \mu\text{m}$
Cantilever Material	Silicon (Si)
Young's Modulus, $E$	$150 \text{ GPa}$ <sup>37</sup>
Density, $D$	$2330 \text{ kg/m}^3$ <sup>38</sup>
Mass, $m$	$4.4736 \times 10^{-12} \text{ kg}$
Spring Constant, $k$	$0.439 \text{ N/m}$
Initial air-gap, $g_o$	$3 \mu\text{m}$
Stopper height, $h_s$	$1.4 \mu\text{m}$
Permittivity of free space, $\epsilon_o$	$8.854 \times 10^{-12} \text{ F/m}$
Ferroelectric material	$SBT (\text{Sr}_{0.8}\text{Bi}_{2.2}\text{Ta}_2\text{O}_9)$ <sup>15</sup>
$\alpha_F$	$-6.5 \times 10^7 \text{ m/F}$
$\beta_F$	$3.75 \times 10^9 \text{ m}^5/\text{F}/\text{C}^2$
$\gamma_F$	$0 \text{ m}^9/\text{F}/\text{C}^4$
Ferroelectric thickness, $t_F$	$5.99 \mu\text{m}$
Ferroelectric area, $A_F$	$1.1659 \times 10^{-12} \text{ m}^2$

The ferroelectric capacitor model is now connected in series with the standalone MEMS model to form the hybrid actuator. Again, the dynamic response of the hybrid actuator (with  $\rho = 0$ ) is obtained by applying a step input voltage as shown in Fig. 6. For the hybrid actuator, the simulation results give a dynamic pull-in voltage  $V_{HDPI}$  of  $0.66 \text{ V}$ , pull-in

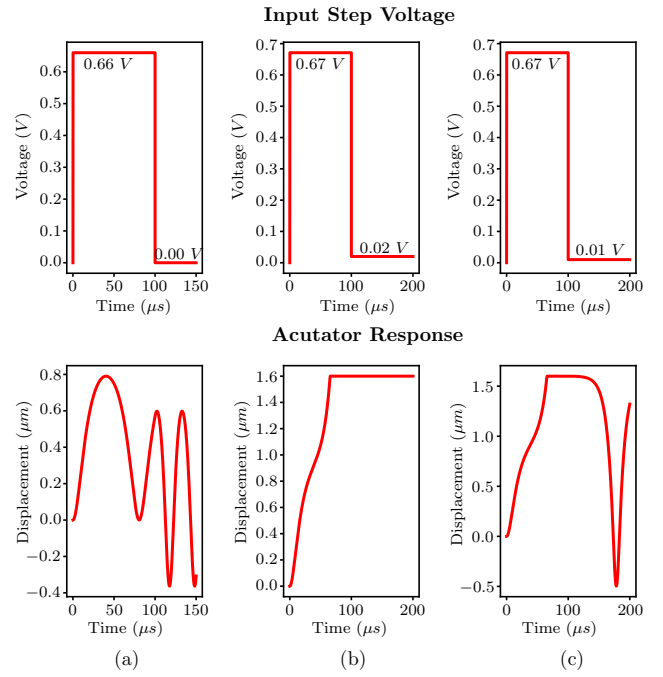


FIG. 6. Ferroelectric negative capacitance - electrostatic MEMS hybrid actuator dynamic response showing significant reduction in operating voltage. (a) Actuator response before dynamic pull-in, showing a reduced dynamic pull-in displacement  $X_{HDPI} = 0.79 \mu\text{m}$ . (b) Actuator response after dynamic pull-in and without release. (c) Actuator response after dynamic pull-in and with release. Note that the pull-in voltage is reduced to  $V_{HDPI} = 0.66 \text{ V}$  and release voltage is reduced to  $V_{HDPO} = 0.01 \text{ V}$ .

displacement  $X_{HDPI}$  of  $0.79 \mu\text{m}$  and release voltage  $V_{HDPO}$  of  $0.01 \text{ V}$ . Compared to the standalone MEMS actuator, there is a significant reduction in the operating voltage of the hybrid actuator. This is because of the voltage amplification due to the negative capacitance of the series ferroelectric capacitor. This sub-1V operation of the hybrid actuator should allow

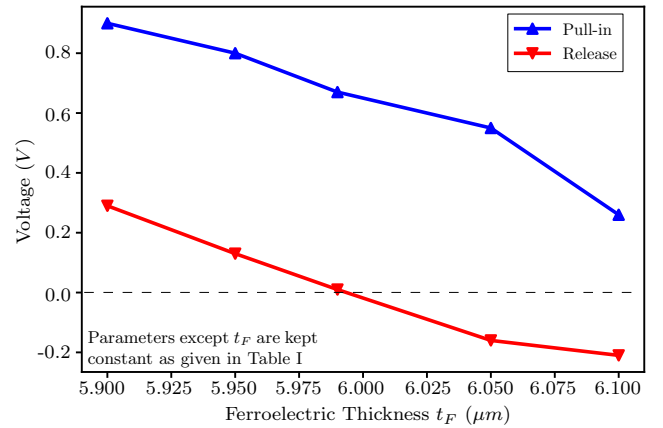


FIG. 7. Effect of ferroelectric thickness  $t_F$  on the dynamic pull-in and release voltages of the hybrid actuator depicting the possibility of obtaining both positive and negative release voltages by proper choice of ferroelectric thickness.

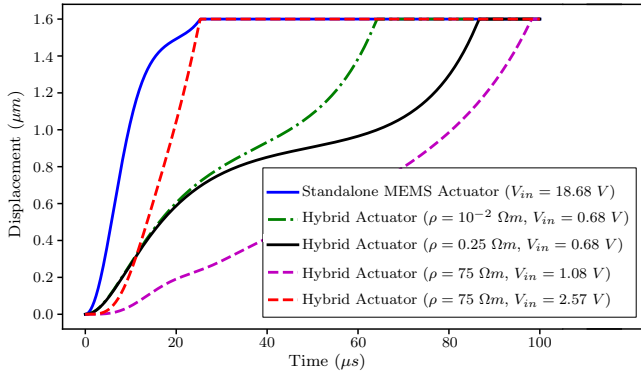


FIG. 8. Dynamic pull-in time analysis of standalone MEMS actuator and hybrid actuator (for different  $\rho$ ). It is shown that the hybrid actuator is slower in comparison with the standalone MEMS actuator to achieve dynamic pull-in. There also exists a trade-off between the applied step voltage and the pull-in time.

seamless integration of such MEMS actuators with modern CMOS devices, eliminating the need for any drive electronics or additional on-chip voltage up-converters. Simulation using SPICE enables a view of the time history response (input vs. time, displacement vs. time) distinctly before & after pull-in and before & after pull-out as shown in Figs. 5 and 6.

### B. Effect of ferroelectric thickness on operating voltage

The effect of ferroelectric thickness  $t_F$  on the dynamic pull-in and release voltages of the hybrid actuator (with  $\rho = 0$ ) is shown in Fig. 7. Increase in the ferroelectric thickness reduces the operating voltage. This is because, with increase in ferroelectric thickness, the ferroelectric capacitance decreases leading to enhanced voltage amplification. This is in agreement with a similar trend observed in ferroelectric negative capacitance - FET (Field Effect Transistor) devices<sup>33</sup> where the gate voltage reduces with increase in ferroelectric thickness. However, the ferroelectric thickness should be properly chosen (i.e.  $|C_F| \sim C_M$ ) so as to preserve the voltage amplification phenomenon. Note that the release voltage can be either positive or negative. Negative release voltage is favorable for bipolar voltage actuation of electrostatic MEMS actuators leading to improved reliability<sup>39,40</sup> and also in memory applications<sup>41</sup>. However, this requires both positive and negative power supplies for operation. Tailoring ferroelectric thickness  $t_F$  can also ensure 0 V release facilitating the use of single sub-1V voltage source for both pull-in and release. For example, a hybrid actuator with  $t_F = 6.10 \mu\text{m}$  has a negative release voltage (-0.21 V), which implies that reducing the applied voltage to 0 V will not result in release. However, a small change in thickness to  $5.95 \mu\text{m}$  (with release voltage 0.13 V) will ensure release of the cantilever at 0 V.

### C. Temporal analysis of dynamic pull-in

A temporal analysis of dynamic pull-in of the standalone MEMS actuator and the hybrid actuator is shown in Fig. 8. The release process is not considered as displacement by only few nanometers is sufficient to release the electrode. Ferroelectric damping, modeled by the resistance  $R_F = \rho t_F / A_F$  in the SPICE model of the ferroelectric capacitor, plays an important role in the time response of the hybrid actuator. A large range of  $\rho$  is used in the simulation for a comprehensive prognosis. The pull-in voltage is a function of  $\rho$ . For each value of the ferroelectric damping constant, a step input voltage 10 mV greater than the pull-in voltage, is used for actuation. It is observed that the hybrid actuator is slower in comparison with the standalone MEMS actuator. However, note that there is a trade-off between the applied step input voltage and the pull-in time – a larger step input voltage will result in faster pull-in of the actuator. This suggests that, by applying a higher step voltage (which is still smaller than that of the standalone actuator), the pull-in time of the hybrid actuator can be made equal to the pull-in time of the standalone actuator. This ensures low-voltage operation of the hybrid actuator without compromising on the pull-in time. For example, both standalone MEMS actuator and hybrid actuator (with  $\rho = 75 \Omega\text{m}$  and step input voltage  $V_{in} = 2.57 \text{ V}$ ) have the same dynamic pull-in time as depicted in Fig. 8.

### D. Effect of ferroelectric damping on energy dissipation

Electrostatic MEMS actuators are inherently low-power devices owing to their near zero power dissipation<sup>42,43</sup>. Reduction in the operating voltage can further reduce the power dissipated during switching and thus enable the use of such actuators in low-power, low-voltage applications. We estimate the energy for pull-in as the time integral of the instantaneous

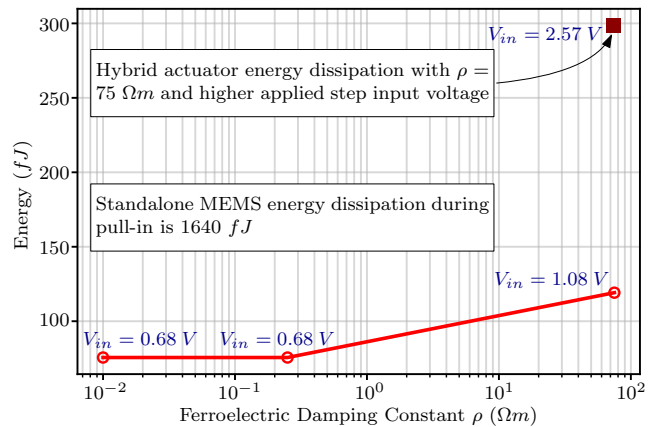


FIG. 9. Effect of ferroelectric damping constant  $\rho$  on the energy dissipation during dynamic pull-in in the hybrid actuator. Note that there is reduction in the energy dissipation in comparison with the standalone MEMS actuator due to reduction in the dynamic pull-in voltage.



power  $v_{in}(t) \cdot i(t)$  over the entire pull-in time. Fig. 9 shows the results of the above calculation. Again, ferroelectric damping constant  $\rho$  plays an important role. As in the case of temporal analysis, we apply a step voltage 10 mV larger than the pull-in voltage in each case to ensure dynamic pull-in. Note that the energy dissipated during pull-in in the standalone MEMS actuator is 1640 fJ. The energy dissipated during pull-in in the hybrid actuator for different values of  $\rho$  varies between 50-150 fJ. For example, for  $\rho = 75 \Omega m$ , the energy dissipated during pull-in is 119.17 fJ. This shows a 10x reduction in the energy dissipation using the hybrid actuator. However, this reduction in energy comes at the cost of slower pull-in. In the previous paragraph, we showed that the actuator can be operated using a voltage higher than pull-in voltage to achieve a pull-in time identical to that of the standalone MEMS actuator. Fig. 9 also shows the energy dissipated when the hybrid actuator with  $\rho = 75 \Omega m$  is actuated with a step voltage  $V_{in} = 2.57 V$ . We find that the energy dissipated is still 5x lower than the energy dissipated in the standalone actuator, indicating a very favorable application of the trade-off between pull-in time and applied voltage.

## V. CONCLUSION

We presented a SPICE based framework to model ferroelectric negative capacitance - electrostatic MEMS hybrid actuator and to analyze the dynamic (step input) response of the hybrid actuator. It is shown that the dynamic pull-in and release voltages of this hybrid actuator are significantly reduced due to the presence of the series ferroelectric capacitor exhibiting negative capacitance. This allows straightforward integration of such actuators with modern CMOS devices. Further, this also opens the door for the use of such actuators in low-power, low-voltage switching applications. The effect of ferroelectric thickness in achieving both positive and negative release voltage is also illustrated. During dynamic pull-in, there is considerable reduction in the energy dissipated in the hybrid actuator as compared to the standalone MEMS actuator, accompanied however by an increase in pull-in time. Nevertheless, we can trade-off pull-in time versus applied voltage to achieve identical pull-in times for the hybrid and standalone actuators and still achieve reduction in the energy dissipated in the hybrid actuator. Finally, since the proposed model is SPICE based and thus circuit compatible, this can be used in combination with other low-voltage CMOS circuits to analyze various heterogeneous CMOS - MEMS systems.

## ACKNOWLEDGMENTS

The authors thank Dr. Revathy Padmanabhan, Dr. Sukomal Dey, Indian Institute of Technology Palakkad, Palakkad and Prof. G. K. Ananthasuresh, Indian Institute of Science, Bengaluru for helpful discussions.

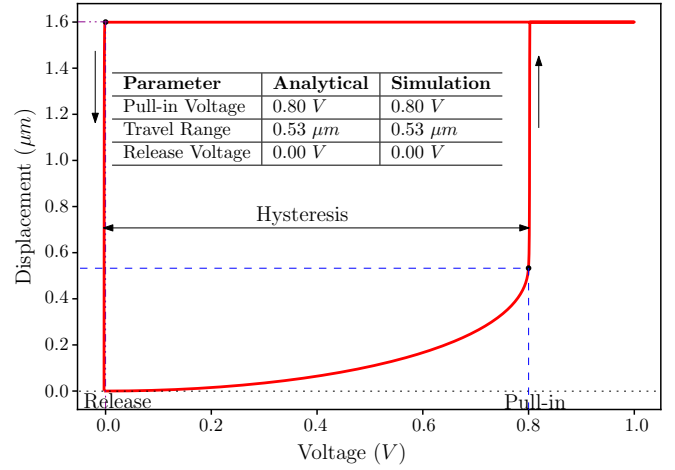


FIG. 10. Static pull-in and release characteristics of the hybrid actuator. The simulation results are in agreement with the analytical results given in Ref. 15, thus validating the hybrid actuator SPICE model.

## Appendix: Static characteristics of the hybrid actuator

The static pull-in voltage  $V_{HSPI}$  and the travel range  $X_{HSPI}$  of the hybrid actuator are given by<sup>15</sup>

$$V_{HSPI} = r_{\alpha N} \sqrt{\frac{r_{\alpha N}}{r_{\beta N}} \cdot \frac{8 k g_o^3}{27 \epsilon_0 A_M}}; X_{HSPI} = \frac{r_{\alpha N}}{r_{\beta N}} \cdot \frac{g_o}{3} \quad (A1)$$

where

$$r_{\alpha N} = 1 - \frac{t_F A_M |\alpha_F| \epsilon_o}{g_o A_F} \quad (A2)$$

$$r_{\beta N} = 1 - \left[ (2 \beta_F k \epsilon_o^2) \left( \frac{t_F A_M^2}{A_F^3} \right) \right] \quad (A3)$$

Assuming zero release voltage, we have  $g_o - h_s = (r_{\alpha N}/r_{\beta N}) g_o$ . Thickness  $t_F$  and area  $A_F$  are designed so as to obtain  $V_{HSPI} = 0.80 V$ . The static pull-in and release characteristics of the hybrid actuator are shown in Fig. 10. The simulation results are in agreement with the analytical results given in Ref. 15, thus validating the hybrid actuator SPICE model.

<sup>1</sup>“2015 International Technology Roadmap for Semiconductors (ITRS),” Tech. Rep. (2015).

<sup>2</sup>M. I. Younis, *MEMS Linear and Nonlinear Statics and Dynamics*, Vol. 20 (Springer US, Boston, MA, 2011).

<sup>3</sup>D. Elata, “On the static and dynamic response of electrostatic actuators,” *Bull. Polish Acad. Sci.* **53**, 373–384 (2005).

<sup>4</sup>K. B. Lee, *Principles of Microelectromechanical Systems* (John Wiley & Sons, 2011).

<sup>5</sup>V. Leus and D. Elata, “On the dynamic response of electrostatic MEMS switches,” *J. Microelectromech. Syst.* **17**, 236–243 (2008).

<sup>6</sup>G. N. Nielson and G. Barbastathis, “Dynamic pull-in of parallel-plate and torsional electrostatic MEMS actuators,” *J. Microelectromech. Syst.* **15**, 811–821 (2006).

<sup>7</sup>L. A. Rocha, E. Cretu, and R. F. Wolffenbuttel, “Pull-in dynamics: Analysis and modeling of the transitional regime,” in *Proc. 17th IEEE Int. Conf. MEMS* (2004) pp. 249–252.

- <sup>8</sup>G. M. Rebeiz, "RF MEMS switches: Status of the technology," in *Proc. 12th Int. Conf. Solid-State Sens., Actuators, Microsyst. (TRANSDUCERS)*, Vol. 2 (2003) pp. 1726–1729.
- <sup>9</sup>N. Dumas, L. Latorre, F. Mailly, and P. Nouet, "Design of a smart CMOS high-voltage driver for electrostatic MEMS switches," in *Symp. Design Test Integration and Packag. of MEMS/MOEMS (DTIP)* (2010) pp. 44–47.
- <sup>10</sup>J. F. Saheb, J. F. Richard, M. Sawan, R. Meingan, and Y. Savaria, "System integration of high voltage electrostatic MEMS actuators," *Analog Integr. Circ. Sig. Process.* **53**, 27–34 (2007).
- <sup>11</sup>J. A. Brandt, *High voltage bias waveform generator for an RF MEMS microswitch*, Master's thesis, University of New Hampshire, Durham (2008).
- <sup>12</sup>J. O. Lee, Y.-H. Song, M.-W. Kim, M.-H. Kang, J.-S. Oh, H.-H. Yang, and J.-B. Yoon, "A sub-1-volt nanoelectromechanical switching device," *Nature Nanotech.* **8**, 36–40 (2013).
- <sup>13</sup>W. W. Jang, J. O. Lee, J.-B. Yoon, M.-S. Kim, J.-M. Lee, S.-M. Kim, K.-H. Cho, D.-W. Kim, D. Park, and W.-S. Lee, "Fabrication and characterization of a nanoelectromechanical switch with 15-nm-thick suspension air gap," *Appl. Phys. Lett.* **92**, 103110 (2008).
- <sup>14</sup>A. Attaran and R. Rashidzadeh, "Ultra low actuation voltage RF MEMS switch," *Micro and Nano Syst. Lett.* **3**, 1–4 (2015).
- <sup>15</sup>M. Masuduzzaman and M. A. Alam, "Effective nanometer airgap of NEMS devices using negative capacitance of ferroelectric materials," *Nano Lett.* **14**, 3160–3165 (2014).
- <sup>16</sup>K. Choe and C. Shin, "Adjusting the operating voltage of an nanoelectromechanical relay using negative capacitance," *IEEE Trans. Electron Devices* **64**, 5270–5273 (2017).
- <sup>17</sup>K. Choe and C. Shin, "Impact of negative capacitance on the energy-delay property of an electromechanical relay," *Jpn. J. Appl. Phys.* **58**, 051003 (2019).
- <sup>18</sup>G. N. Nielson, R. H. Olsson, G. R. Bogart, P. R. Resnick, O. B. Spahn, C. Tigges, G. Grossetete, and G. Barbastathis, "Dynamic pull-in and switching for sub-pull-in voltage electrostatic actuation," in *Proc. 14th Int. Conf. Solid-State Sens., Actuators, Microsyst. (TRANSDUCERS)* (2007) pp. 455–459.
- <sup>19</sup>S. Shekhar, K. J. Vinoy, and G. K. Ananthasuresh, "Switching and release time analysis of electrostatically actuated capacitive RF MEMS switches," *Sens. Transducers* **130**, 77–90 (2011).
- <sup>20</sup>G. M. Rebeiz, *RF MEMS: Theory, Design, and Technology* (John Wiley & Sons, 2004).
- <sup>21</sup>H. Toshiyoshi, "A SPICE-based multi-physics simulation technique for integrated MEMS," in *IEEE Int. Conf. Simulation of Semiconductor Processes and Devices* (2011) pp. 239–242.
- <sup>22</sup>A. Vladimirescu, *The SPICE book* (John Wiley & Sons, Inc., 1994).
- <sup>23</sup>R. Vogelsong and C. Brzezinski, "Extending SPICE for electro-thermal simulation," in *1989 Proceedings of the IEEE Custom Integrated Circuits Conference* (IEEE, 1989) pp. 21–4.
- <sup>24</sup>J. Chavez, J. Ortega, J. Salazar, A. Turo, and M. J. Garcia, "SPICE model of thermoelectric elements including thermal effects," in *Proceedings of the 17th IEEE Instrumentation and Measurement Technology Conference [Cat. No. 00CH37066]*, Vol. 2 (IEEE, 2000) pp. 1019–1023.
- <sup>25</sup>J. M. Xu and D. S. Ellis, "OE UT-spice: a CAD tool for design and simulation of OEIC," in *Optoelectronic Integrated Circuits*, Vol. 3006 (International Society for Optics and Photonics, 1997) pp. 406–418.
- <sup>26</sup>L. Ravezzi, G.-F. Dalla Betta, D. Stoppa, and A. Simoni, "A versatile photodiode SPICE model for optical microsystem simulation," *Microelectronics journal* **31**, 277–282 (2000).
- <sup>27</sup>W. M. Leach, "Controlled-source analogous circuits and SPICE models for piezoelectric transducers," *IEEE Transactions on ultrasonics, ferroelectrics, and frequency control* **41**, 60–66 (1994).
- <sup>28</sup>M. Madec, C. Lallement, and J. Haiech, "Modeling and simulation of biological systems using SPICE language," *PLoS one* **12**, e0182385 (2017).
- <sup>29</sup>H. Takao, M. Sugiura, M. Ishida, K. Terao, T. Suzuki, F. Shimokawa, and F. Oohira, "Micro fluidic circuit design with "spice" simulation," in *2011 IEEE 24th International Conference on Micro Electro Mechanical Systems (IEEE, 2011)* pp. 1154–1157.
- <sup>30</sup>S. Salahuddin and S. Datta, "Use of negative capacitance to provide voltage amplification for low power nanoscale devices," *Nano Lett.* **8**, 405–410 (2008).
- <sup>31</sup>A. I. Khan, K. Chatterjee, B. Wang, S. Drapcho, L. You, C. Serrao, S. R. Bakaul, R. Ramesh, and S. Salahuddin, "Negative capacitance in a ferroelectric capacitor," *Nature Mater.* **14**, 182–186 (2015).
- <sup>32</sup>A. Aziz, S. Ghosh, S. Datta, and S. K. Gupta, "Physics-based circuit-compatible SPICE model for ferroelectric transistors," *IEEE Electron Device Lett.* **37**, 805–808 (2016).
- <sup>33</sup>Y. Li, K. Yao, and G. S. Samudra, "Delay and power evaluation of negative capacitance ferroelectric MOSFET based on SPICE model," *IEEE Trans. Electron Devices* **64**, 2403–2408 (2017).
- <sup>34</sup>Y. Li, Y. Kang, and X. Gong, "Evaluation of negative capacitance ferroelectric MOSFET for analog circuit applications," *IEEE Trans. Electron Devices* **64**, 4317–4321 (2017).
- <sup>35</sup>A. I. Khan, *Negative Capacitance for Ultra-Low Power Computing*, Ph.D. thesis, UC Berkeley (2015).
- <sup>36</sup>M. Pešić, C. Künneth, M. Hoffmann, H. Mulaosmanovic, S. Müller, E. T. Breyer, U. Schroeder, A. Kersch, T. Mikolajick, and S. Slesazek, "A computational study of hafnia-based ferroelectric memories: from ab initio via physical modeling to circuit models of ferroelectric device," *J. Comput. Electron.* **16**, 1236–1256 (2017).
- <sup>37</sup>J. Kim, D. D. Cho, and R. S. Muller, "Why is (111) silicon a better mechanical material for MEMS?" in *Transducers' 01 Eurosensors XV* (Springer, 2001) pp. 662–665.
- <sup>38</sup>J. F. Shackelford, Y.-H. Han, S. Kim, and S.-H. Kwon, *CRC Materials Science and Engineering Handbook* (CRC press, 2016).
- <sup>39</sup>Z. Peng, X. Yuan, J. C. Hwang, D. I. Forehand, and C. L. Goldsmith, "Dielectric charging of RF MEMS capacitive switches under bipolar control-voltage waveforms," in *Proc. IEEE/MTT-S Int. Microw. Symp.* (2007) pp. 1817–1820.
- <sup>40</sup>M. Domínguez, D. López, D. Molinero, and J. Pons-Nin, "Dielectric charging control for electrostatic MEMS switches," in *Proc. SPIE*, Vol. 7679 (2010) pp. 1–11.
- <sup>41</sup>W. Y. Choi, T. Osabe, and T.-J. K. Liu, "Nano-Electro-Mechanical non-volatile memory (NEMory) cell design and scaling," *IEEE Trans. Electron Devices* **55**, 3482–3488 (2008).
- <sup>42</sup>E. R. Brown, "RF-MEMS switches for reconfigurable integrated circuits," *IEEE Trans. Microw. Theory Tech.* **46**, 1868–1880 (1998).
- <sup>43</sup>G. M. Rebeiz and J. B. Muldavin, "RF MEMS switches and switch circuits," *IEEE Microw. Mag.* **2**, 59–71 (2001).